58918-00-105

Conference Paper

Jahn-Teller Splitting and Zeeman Effect of Acceptors in Diamond

Hyunjung Kim,[a,*] S. Rodriguez,[a] M. Grimsditch,[b] T. R. Anthony,[c] and A.K. Ramdas[a]

[a]*Department of Physics, Purdue University, West Lafayette, IN 47907-1396*

[b]*Materials Science Division, Argonne National Laboratory, Argonne, IL 60439*

[c]*General Electric Company Corporate Research and Development, Schenectady, NY 12309*

The 20th International Conference on Defects in Semiconductors, The University of California at Berkeley, Berkeley, CA, July 26-30, 1999

Work supported by the U.S. Department of Energy, Basic Energy Sciences-Materials Science under contract #W-31-109-ENG-38 at Argonne and from the National Science Foundation Grant No. DMR 98-00858 at Purdue.

*Present address: Advanced Photon Source, Argonne National Laboratory, Argonne, IL 60439.

DISCLAIMER

The 20th International Conference on Defects in Semiconductors, July 26-30, 1999, The University of California at Berkeley, Berkeley, CA.

Jahn-Teller splitting and Zeeman effect of acceptors in diamond

Hyunjung Kim[a*], S. Rodriguez[a], M. Grimsditch[b], T. R. Anthony[c], and A. K. Ramdas[a]

[a] *Department of Physics, Purdue University, West Lafayette, IN 47907, USA*

[b] *Argonne National Laboratory, Argonne, IL 60439, USA*

[c] *GE Corp. Research and Development, Schenectady, NY 12309, USA*

(July 18, 1999)

Abstract

Employing the high resolution of a 5+4 tandem Fabry-Pérot interferometer, we discovered that Δ', the Raman active electronic transition between the spin-orbit split $1s(p_{3/2}) : \Gamma_8$ and $1s(p_{1/2}) : \Gamma_7$ acceptor ground states, is a doublet for a boron impurity in diamond with a clearly resolved spacing of 0.81 ± 0.15 cm^{-1}. The direct observation of a Stokes/anti-Stokes pair with 0.80 ± 0.04 cm^{-1} shift provides a striking confirmation that the lower $1s(p_{3/2}) : \Gamma_8$ ground state has experienced a splitting due to a static Jahn-Teller distortion. The Zeeman effect of Δ' has been investigated with a magnetic field along several crystallographic directions. Theory of the Zeeman effect, formulated in terms of the symmetry of the substitutional acceptor and the Luttinger parameters of the valence band, allows quantitative predictions of the relative intensities of the Zeeman components in full agreement with experiments. The observation of transitions *within* the Γ_8 Zeeman multiplet, i.e., the Raman-electron-paramagnetic-resonances, is yet another novel feature to emerge from the present study. The investigation has also yielded g-factors characterizing the Zeeman multiplets.

Keywords: Jahn-Teller splitting, Zeeman effect, acceptors, diamond

Name and contact information of corresponding author:

Hyunjung Kim

Department of Physics

Purdue University

West Lafayette, IN 47907

USA

Ph. 765-494-3020

Fax 765-494-0706

e-mail: hjk@physics.purdue.edu

Current address:

Advanced Photon Source

Argonne National Laboratory

Argonne, IL 60439

USA

Ph. 630-252-9141

Fax 630-252-3222

e-mail: hjk@aps.anl.gov

I. INTRODUCTION

Bound states of electrons (holes) bound to Coulomb centers represented by substitutional group V (group III) impurities in group IV semiconductors, with small binding energies and extended wavefunctions (and hence labeled "shallow" centers), are successfully described in the effective mass theory (EMT) [1,2]. The screened Coulomb potential; the effective mass parameters and the symmetry of the band extremum with which the electronic states are associated; and the site symmetry of the impurity—these are the basic ingredients of EMT. To the extent the wavefunctions of the bound states probe the immediate vicinity of the impurity, as those of the $1s$-like ground state of these solid state ánalogs of the H-atom, relevant corrections to EMT are introduced. In the context of such considerations, the case of substitutional boron acceptors in diamond (in the so called type IIb, blue diamonds) is particularly fascinating in view of distinctive underlying features: the largest departure from the spherical approximation [3] exhibited by any of the tetrahedrally coordinated semiconductors and the small spin-orbit splitting of the valence band. Spectroscopic investigations of the electronic states of holes bound to boron acceptors are particularly tractable thanks to its successful incorporation in sufficient concentrations in man-made diamonds [4–6], besides its occurrence in extremely rare natural specimens [7].

We recently reported the electronic Raman line associated with the transition between the spin-orbit split $1s$ ground states i.e., the $1s(p_{3/2}) : \Gamma_8 \rightarrow 1s(p_{1/2}) : \Gamma_7$ (labeled Δ') in boron doped diamonds with natural isotopic composition as well as in a ^{13}C specimen [5,6]. In this paper we present the results of a high resolution investigation of the Δ' line of boron-doped diamond employing a tandem Fabry-Pérot interferometer. Further, we have fully characterized Δ' with its Zeeman splitting and the polarizations of the Zeeman components which have yielded insights into the mass anisotropy of the valence band maximum and the g-factors for the participating levels.

II. THE Δ' LINE WITHOUT PERTURBATION

The energy levels of a hole bound to a boron acceptor in diamond are shown schematically in the inset to Fig. 1. The effective mass ground state shows a spin-orbit splitting into $1s(p_{3/2}) : \Gamma_8$ and $1s(p_{1/2}) : \Gamma_7$ states, separated by Δ' corresponding to Δ, the spin-orbit splitting of the valence band maximum. Also shown are the Lyman transitions originating from the $1s(p_{3/2})$ and $1s(p_{1/2})$ ground states. The transition *between* the two $1s$ ground states is strongly Raman allowed but infrared forbidden due to the approximate even parity of both levels.

In order to study the Δ' transition with precision as well as with the ability to observe small shifts, we resorted to a 5+4 tandem, piezo-electrically scanned Fabry-Pérot interferometer. We discovered that it is actually a doublet with a separation of 0.81 ± 0.15 cm^{-1} as shown in Fig. 1. Note that the lower electronic ground state, $1s(p_{3/2}) : \Gamma_8$ is four fold degenerate; as such, it is a prime candidate for a Jahn-Teller splitting into two Kramers doublets. We ensured that the doublet structure did not originate in the procedure adopted for mounting the diamond specimen. We observed it in four blue diamonds with natural isotopic composition; within experimental accuracy, the splittings are same in all the samples and in different crystallographic directions. Random strains introduced during crystal growth are not expected to be homogeneous and the same from specimen to specimen; thus they cannot produce identical splittings but will cause only broadening and hence can be ruled out as the origin of the splitting.

We have explored both static and dynamic Jahn-Teller effect as the microscopic underlying mechanisms for the above splitting [8] and concluded that the static Jahn-Teller approach provides a physically meaningful interpretation. A group theoretical analysis, taken together with the experimental results including polarization effects, shows that the $1s(p_{3/2} : \Gamma_8)$ level experiences a distortion along a cubic axis and splits it into $\psi_{\pm 3/2}$ and $\psi_{\pm 1/2}$ levels. It is specially significant that near ω_L, the unshifted exciting laser frequency, two new features identified with a star appear; they occur with a frequency shift of 0.80 ± 0.04 cm^{-1} from ω_L

equal to the Jahn-Teller splitting of Δ'. We interpret them as the Stokes and the anti-Stokes Raman line corresponding to the transition *within* the Jahn-Teller split $1s(p_{3/2})$ levels i.e., it corresponds to the $\psi_{\pm 3/2} \rightarrow \psi_{\pm 1/2}$ transition. To our knowledge this is the smallest Raman shift ever reported in the literature other than those of Brillouin components.

III. THE ZEEMAN EFFECT OF Δ'

The Zeeman effect of the Δ' Raman line, in an external magnetic field $\mathbf{B}$ of 4 T along $\mathbf{z}||[001]$ and the sample temperature of 5.3 K, is displayed in Fig. 2. The Raman spectrum, recorded with the tandem Fabry-Pérot interferometer in the right angle scattering geometry $\mathbf{y}(\mathbf{zx}+\mathbf{zy})\mathbf{z}$ where $\mathbf{x}$, $\mathbf{y}$, and $\mathbf{z}$ are the cubic axes, shows four fully resolved Zeeman components of Δ' labeled 1′, 2′, 3′, and 4′. With incident light along $\mathbf{y}$ and polarized along $\mathbf{z}$ and the scattered light unanalyzed, the experiment allows the $\mathbf{zx}$ and $\mathbf{zy}$ components of the Raman tensors of the Zeeman transitions to appear [9].

The inset to Fig. 2 shows schematically the four sublevels of $1s(p_{3/2}) : \Gamma_8$ and two of $1s(p_{1/2}) : \Gamma_7$ for $\mathbf{B} \neq 0$. (The figure is appropriate for magnetic fields in which the Jahn-Teller splitting can be neglected in comparison to the Zeeman splitting.) The ordering of the Zeeman sublevels of the two $1s$ states is based on the polarization features of the Zeeman components and the negative sign for the g-factor of free hole i.e., from an appeal to the experimental observations: The selection rules for the Zeeman transitions are: $\delta = m - M = 0, \pm 2$ for the transitions 1, 2, 3, and 4 while $\delta = \pm 1$ apply to 1′, 2′, 3′, and 4′, the Zeeman components observed under the experimental conditions of Fig. 2. Here $m = \pm 1/2$ denote the magnetic quantum numbers of the $1s(p_{1/2})$ level while $M = \pm 3/2$ and $\pm 1/2$ those of the $1s(p_{3/2})$ [9].

In Fig. 2, in addition to the Zeeman components of Δ', and the intrinsic transverse acoustic (TA) and longitudinal acoustic (LA) Brillouin components, two Stokes/anti-Stokes pairs labeled $E1'$ and $E2'$ with significantly smaller shifts can be observed. They correspond to the electron-paramagnetic-resonances (Raman-EPR transitions) *within* the Zeeman mul-

tiplet of $1s(p_{3/2})$ satisfying $\Delta M = \pm 1$. In the linear approximation for the Zeeman effect, the sublevels of $1s(p_{3/2})$ are spaced equally leading to identical energies for the $E1'$ and $E2'$ lines. The experimental observation thus unambiguously shows the contribution of Zeeman energies quadratic in $\mathbf{B}$ making the spacings unequal [9]. The $\psi_{\pm 1/2} \rightarrow \psi_{\mp 1/2}$ as well as the $\psi_{\pm 3/2} \rightarrow \psi_{\mp 3/2}$ EPR transitions are forbidden by time-reversal symmetry in Raman effect.

The Zeeman effect of Δ' for $\mathbf{B}||[110]$, employing a charge-coupled-device (CCD) based triple grating spectrometer, is displayed in Fig. 3. It is recorded with incident radiation along $\mathbf{z}||[001]$, polarized along $\mathbf{y}'||[\bar{1}10]$ or $\mathbf{x}'||[110]$, and scattered along $\mathbf{x}'$, analyzed along $\mathbf{z}$ or $\mathbf{y}'$. The polarization configurations accessible in this right angle scattering geometry allows the $\mathbf{x}'\mathbf{z}$, $\mathbf{x}'\mathbf{y}'$, $\mathbf{y}'\mathbf{y}'$, and $\mathbf{y}'\mathbf{z}$ components of the Raman polarizability tensors to be observed. It can be shown [9] that level scheme in the inset to Fig. 2 applies equally to this case for a given $\mathbf{B}$; hence $1'$, $2'$, $3'$, and $4'$ can appear in $\mathbf{z}(\mathbf{x}'\mathbf{z})\mathbf{x}'$, $\delta = \pm 1$, Fig. 3(a), whereas 1, 2, 3, and 4 can be seen in $\mathbf{z}(\mathbf{y}'\mathbf{y}')\mathbf{x}'$ conforming to $\delta = 0, \pm 2$, Fig. 3(b). Thus one can deduce the distinct but small separation between the primed and the unprimed components, $(1, 1')$, $(2, 2')$, $(3, 3')$, and $(4, 4')$, i.e., the splitting of the $1s(p_{1/2}) : \Gamma_7$ level. The significantly larger splittings of the $1s(p_{3/2}) : \Gamma_8$ level are obtained from similar comparisons of spacings between 1 and $2'$ and $1'$ and 2 yielding the $(-1/2, -3/2)$ separation while the $(1/2, -1/2)$ and $(3/2, 1/2)$ intervals are given by the spacings of $(2, 3')$, $(2', 3)$ and $(3, 4')$, $(3', 4)$, respectively [9]. The $(\mathbf{x}'\mathbf{y}')$ polarization permits the observation of $1'$, $2'$, $3'$, and $4'$ but their conspicuous absence in Fig. 3(c) is due to their intensities being proportional to γ_2^2, where the γ_2 Luttinger parameter is an order of magnitude smaller than γ_3 [6], the Luttinger parameter which essentially controls the Raman intensities in Fig. 3(a), 3(b), and 3(d).

IV. g-FACTORS

On the basis of the magnetic field dependence of the Zeeman components of Δ' and of the Raman-EPR lines, $g_{3/2}$ and $g_{1/2}$, the g-factors characteristic of $1s(p_{3/2})$ and $1s(p_{1/2})$ can be obtained. It can be shown that the $J = 3/2$ and $J = 1/2$ "angular momentum"

states split into $g_{3/2}\mu_B BM$ and $g_{1/2}\mu_B Bm$, respectively. Here μ_B is the Bohr magneton, $g_{3/2} = \frac{1}{3}(2g_1 + g_2)$ and $g_{1/2} = \frac{1}{3}(4g_1 - g_2)$, g_1 and g_2 are the g-factors for the orbital and spin-angular momenta, respectively [9]. The magnetic field dependence of the energies of the Zeeman components of Δ' yield $g_{3/2} = -0.94 \pm 0.02$ and $g_{1/2} = 0.16 \pm 0.05$; in turn they lead to $g_1 = -0.39 \pm 0.04$ and $g_2 = -2.04 \pm 0.10$.

V. CONCLUDING REMARKS

While Si and Ge, the other two elemental group IV semiconductors, have been intensively investigated in the context of shallow donors and acceptors, the corresponding studies in diamond could not be pursued with equal effort . The main bottleneck has been the limited and sporadic successes in the incorporation of dopants; until recently the technological challenges remained daunting. The case of boron acceptors in diamond shows how insightful spectroscopic techniques can be exploited when appropriately doped specimen become available. The studies on boron acceptors in diamond shows in a particularly striking manner the power of Raman techniques when applied to Lyman spectroscopy; they provide information complementary to that obtained from infrared. Finally, the high resolution and the freedom from parasitic radiation of a tandem Fabry-Pérot interferometer; the optical quality of diamond which makes it exceptionally suited for spectroscopy; and the electronic band structure with unusual features are some of the unique aspects of diamond in the context of impurity states of semiconductors.

ACKNOWLEDGMENTS

The authors acknowledge support from the National Science Foundation Grant No. DMR 98-00858 at Purdue University and from the U.S. Department of Energy, BES Material Sciences (Grant No. W-31-109-ENG-38) at Argonne National Laboratory.

REFERENCES

* Present address: Advanced Photon Source, Argonne National Laboratory, Argonne, IL 60439.

[1] W. Kohn, in: *Solid State Physics*, ed. F. Seitz and D. Turnbull (Academic, New York, 1957), vol. 5, p. 257.

[2] A. K. Ramdas and S. Rodriguez, Rep. Prog. Phys. **44** (1981) 1297.

[3] A. Balderschi and N. O. Lipari, Phys. Rev. B **8** (1973) 2697; *ibid* **9** (1974) 1525. These authors have introduced valence band parameters $\mu = 2(3\gamma_3+2\gamma_2)/5\gamma_1$ and $\delta = (\gamma_3-\gamma_2)/\gamma_1$ where γ_1, γ_2, and γ_3 are the Luttinger parameters; μ measures the strength of spherically symmetric contributions to the light and heavy hole kinetic energy while δ gives the deviation of the hole energies from sphericity. Among the tetrahedrally coordinated elemental group IV and the III-V and II-VI semiconductors, (μ/δ) has the *smallest* value for diamond. We have used the γ_1, γ_2, γ_3 values of L. Reggiani, D. Waechter, and S. Zukotynski, Phys. Rev. B **28** (1983) 3550.

[4] H. Kim, A. K. Ramdas, S. Rodriguez, and T. R. Anthony, Solid State Commun. **102** (1997) 861.

[5] H. Kim, R. Vogelgesang, A. K. Ramdas, S. Rodriguez, M. Grimsditch, and T. R. Anthony, Phys. Rev. Lett. **79** (1997) 1706.

[6] H. Kim, R. Vogelgesang, A. K. Ramdas, S. Rodriguez, M. Grimsditch, and T. R. Anthony, Phys. Rev. B **57** (1998) 15315.

[7] J. F. H. Custers, Physica **18** (1952) 489; *ibid* **20** (1954) 183.

[8] H. Kim, A. K. Ramdas, S. Rodriguez, M. Grimsditch, and T. R. Anthony, (unpublished).

[9] H. Kim, A. K. Ramdas, S. Rodriguez, M. Grimsditch, and T. R. Anthony, (unpublished).

FIGURES

FIG. 1. The Δ' line as a Jahn-Teller doublet, the transition between the Jahn-Teller split $1s(p_{3/2})$ levels, labeled with a star ($\star$), and the intrinsic transverse acoustic (TA) and longitudinal acoustic (LA) Brillouin components in the scattered light from a natural type IIb diamond spectrally analyzed with a high resolution tandem Fabry-Pérot interferometer. The spectrum is recorded in the right angle scattering geometry $\mathbf{z}(\mathbf{y'y'} + \mathbf{y'z})\mathbf{x'}$; here $\mathbf{x'}||[110]$, $\mathbf{y'}||[\bar{1}10]$ and $\mathbf{z}||[001]$ and the incident light along $\mathbf{z}$ is polarized along $\mathbf{y'}$ whereas the scattered light along $\mathbf{x'}$ is not analyzed. The wavelength of the exciting laser radiation (λ_L) is 5145 Å (Ar^+). ω_L is the unshifted laser frequency and G identifies its 'ghosts' due to leakage in the tandem operation. The inset shows energy levels of a hole bound to a substitutional boron acceptor in diamond. The Jahn-Teller split $1s(p_{3/2})$ levels and the transition between them, identified with a star ($\star$), and the two transitions resulting in the Δ' line as a doublet are shown in the enlarged view presented within the circle. V. B. $\equiv$ Valence Band.

FIG. 2. The Zeeman splitting of the Δ' electronic Raman transition of a boron acceptor in a man-made type IIb diamond recorded with the tandem Fabry-Pérot interferometer. The experiment was carried out with: a 4 T magnetic field (B) along [001]; temperature, T=5.3 K; and $\lambda_L = 5145$ Å line of Ar^+ laser. The spectra are recorded in the right-angle scattering geometry, $\mathbf{y}(\mathbf{zx} + \mathbf{zy})\mathbf{z}$; $\mathbf{x}$, $\mathbf{y}$, and $\mathbf{z}$ are along [100], [010], and [001], respectively; ω_L, G, TA, and LA are defined in Fig. 1. The Zeeman components are labeled according to the inset.

FIG. 3. The polarization features of the Zeeman components of Δ' of a natural type IIb diamond for $\mathbf{B}||[110]$, recorded in a right-angle scattering geometry in which incident light is along $\mathbf{z}$, polarized along $\mathbf{y'}$ or $\mathbf{x'}$, and scattered parallel to $\mathbf{x'}$, analyzed along $\mathbf{z}$ or $\mathbf{y'}$. Here $\mathbf{x'}||[110]$, and $\mathbf{y'}||[\bar{1}10]$. The spectral analysis was performed with a CCD-based triple grating spectrometer; $\lambda_L = 6471$ Å (Kr^+) laser. The Zeeman components are labeled 1, 1′; 2, 2′; 3, 3′; and 4, 4′ following the energy level scheme shown in the inset of Fig. 2. The feature labeled with a '+' mark is of unknown origin.

Fig. 1

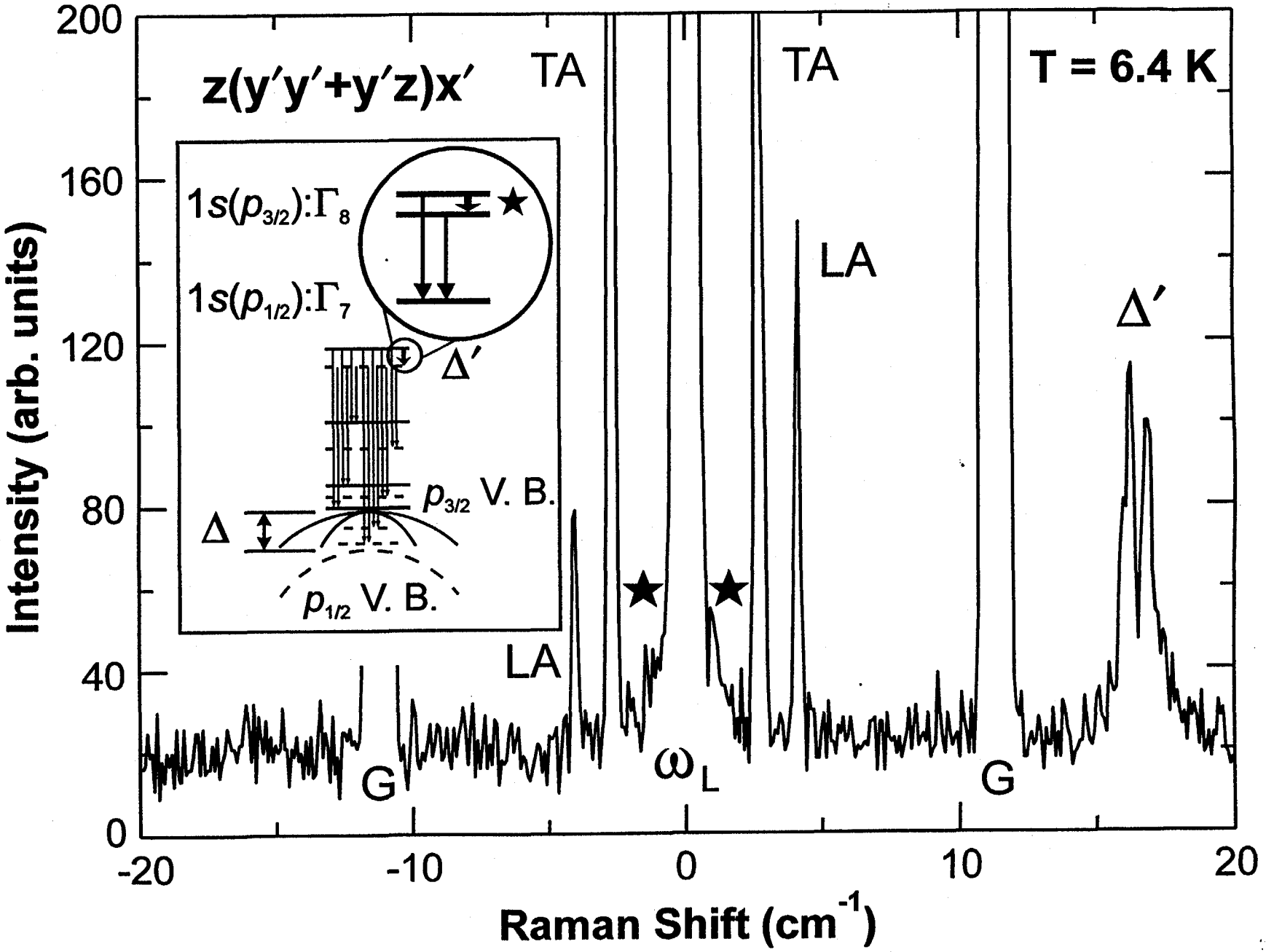
z(y′y′+y′z)x′
TA
TA
T = 6.4 K
LA
Δ′
LA
G
ω_L
G
1s(p_3/2):Γ_8
1s(p_1/2):Γ_7
Δ′
p_3/2 V. B.
Δ
p_1/2 V. B.
Intensity (arb. units)
Raman Shift (cm^-1)
200
160
120
80
40
0
-20
-10
0
10
20

Fig. 2

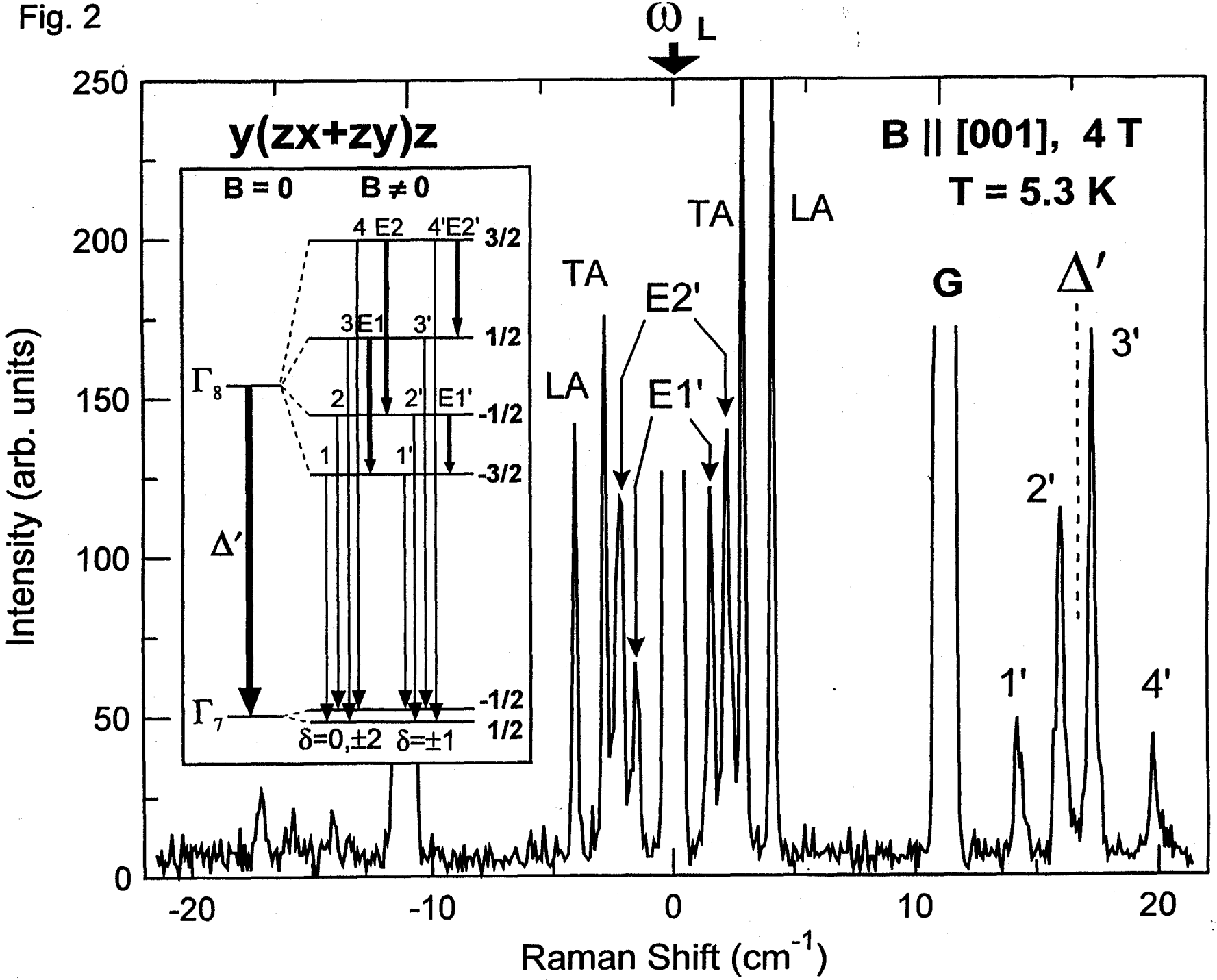
ω L
y(zx+zy)z
B || [001], 4 T
T = 5.3 K
B = 0
B ≠ 0
4 E2
4'E2'
3/2
3E1
3'
1/2
Γ8
2
2'
E1'
-1/2
1
1'
-3/2
Δ′
Γ7
-1/2
1/2
δ=0,±2
δ=±1
TA
LA
TA
LA
E2'
E1'
G
Δ′
3'
2'
1'
4'
Intensity (arb. units)
250
200
150
100
50
0
-20
-10
0
10
20
Raman Shift (cm-1)

Fig. 3

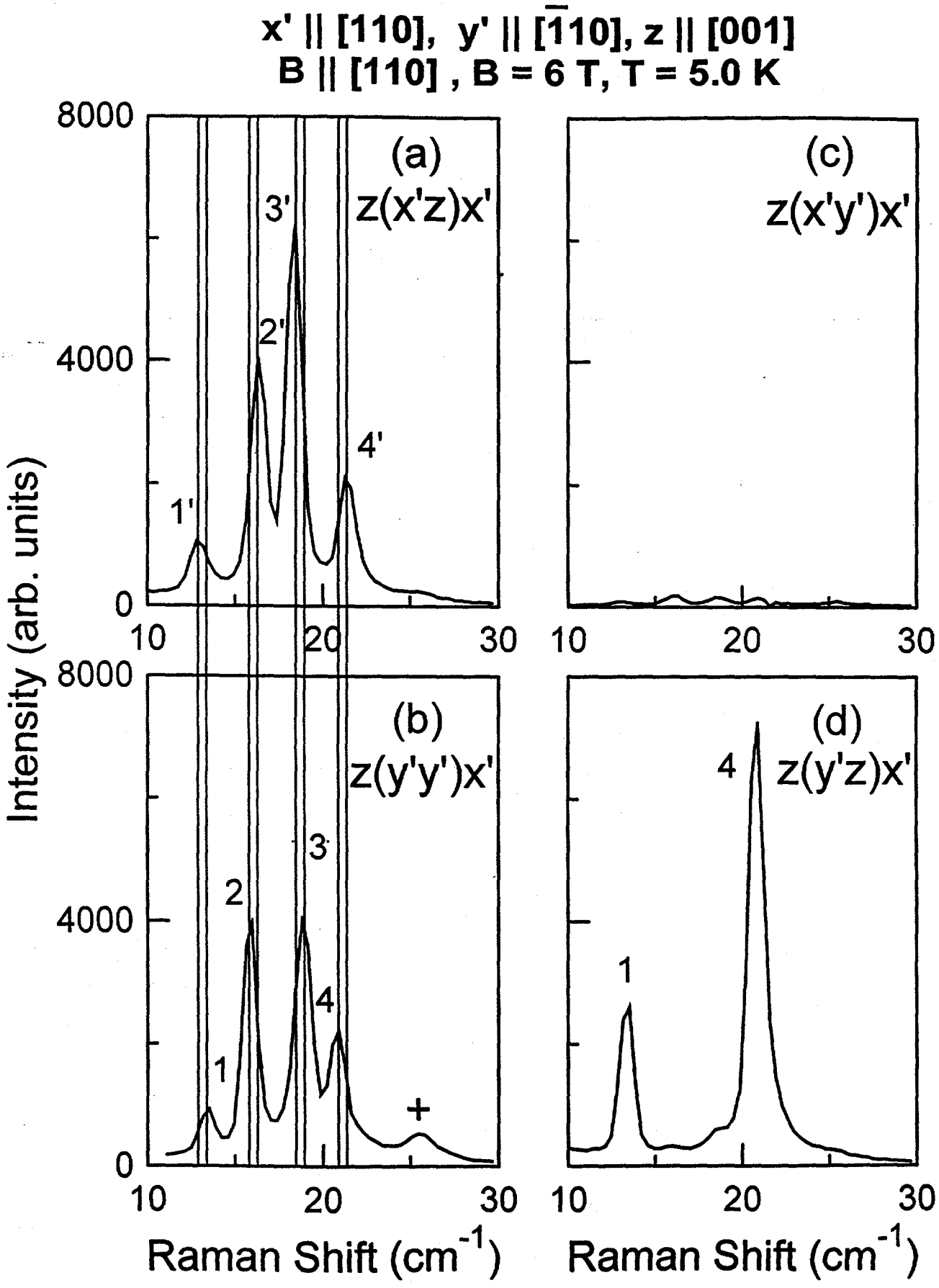
x' || [110], y' || [$\bar{1}$10], z || [001]
B || [110] , B = 6 T, T = 5.0 K
(a)
z(x'z)x'
(c)
z(x'y')x'
(b)
z(y'y')x'
(d)
z(y'z)x'
1'
2'
3'
4'
1
2
3
4
+
8000
4000
0
10
20
30
Intensity (arb. units)
Raman Shift (cm^{-1})
Raman Shift (cm^{-1})